Manifestation of coherent magnetic anisotropy in a carbon nanotube matrix with low ferromagnetic nanoparticle content

2015 New J. Phys. 17 023073

(http://iopscience.iop.org/1367-2630/17/2/023073)

New Journal of Physics
The open access journal at the forefront of physics

Deutsche Physikalische Gesellschaft DPG
IOP Institute of Physics

Published in partnership with: Deutsche Physikalische Gesellschaft and the Institute of Physics

OPEN ACCESS

RECEIVED
14 July 2014

REVISED
29 September 2014

ACCEPTED FOR PUBLICATION
29 January 2015

PUBLISHED
24 February 2015

PAPER

Manifestation of coherent magnetic anisotropy in a carbon nanotube matrix with low ferromagnetic nanoparticle content

A L Danilyuk[1], I V Komissarov[1], V A Labunov[1], F Le Normand[2], A Derory[3], J M Hernandez[4], J Tejada[4] and S L Prischepa[1]

[1] Belarusian State University of Informatics and Radioelectronics, P. Browka 6, Minsk 220013, Belarus
[2] Laboratory of Engineering, Informatics and Imagery (ICube) - Départment Electronique des Solides, des Systèmes et de Photonique (DESSP), Université de Strasbourg and CNRS, Bat. 28, 23 Rue du Loess, BP 20 CR, 67037, Strasbourg Cedex 2, France
[3] Institut de Physique et Chimie des Matériaux (IPCMS), Université de Strasbourg and CNRS, Bat. 69, 23 rue du Loess, BP 43, 67034 Strasbourg Cedex 2, France
[4] Departament de Física Fonamental, Facultat de Física, Universitat de Barcelona, Avinguda Diagonal 645, 08028 Barcelona, Spain

E-mail: prischepa@bsuir.by

Keywords: magnetic nanocomposite, carbon nanotubes, random anisotropy model, law of the approach to saturation, coherent magnetic anisotropy

Abstract

The influence of the magnetic medium can lead to peculiar interaction between ferromagnetic nanoparticles (NPs). Most research in this area involves analysis of the interplay between magnetic anisotropy and exchange coupling. Increasing the average interparticle distance leads to the dominant role of the random magnetic anisotropy. Here we study the interparticle interaction in a carbon nanotube (CNT) matrix with low ferromagnetic NP content. Samples were synthesized by floating catalyst chemical vapor deposition. We found that below some critical NP concentration, when NPs are intercalated only inside CNTs, and at low temperatures, the extended magnetic order, of up to 150 nm, presents in our samples. It is shown by analyzing the correlation functions of the magnetic anisotropy axes that the extended order is not simply due to random anisotropy but is associated with the coherent magnetic anisotropy, which is strengthened by the CNT alignment. With increasing temperature the extended magnetic order is lost. Above the critical NP concentration, when NPs start to be intercalated not only into inner CNT channels, but also outside CNTs, the coherent anisotropy weakens and the exchange coupling dominates in the whole temperature range. We can make a connection with the various correlation functions using the generalized expression for the law of the approach to saturation and show that these different correlation functions reflect the peculiarities in the interparticle interaction inside CNTs. Moreover, we can extract such important micromagnetic parameters like the exchange field, local fields of random and coherent anisotropies, as well as their temperature and NP concentration dependencies.

1. Introduction

Magnetic nanocomposites are currently the subject of intensive studies. Interest in them is associated with the possibility of their potential applications in various fields of magnetoelectronics [1, 2], biology and biomedicine [3, 4], in particular, for the treatment of cancer tumors [5]. At the same time, magnetic nanocomposites are still very attractive objects in fundamental physics because their magnetic properties are determined basically by the nanoscale size of magnetic nanoparticles (NPs). The matrix material of the nanocomposite, into which magnetic NPs are introduced, could also significantly influence all of the magnetic properties. Actually, matrix materials like polymers [6], silica [7], porous silicon [8], and carbon nanotubes (CNT) [9] are widely used nowadays. NPs are introduced into the matrix material in various ways, like co-precipitation, thermal decomposition, hydrothermal synthesis [10], co-evaporation and co-sputtering [6], laser ablation [11], electrochemical

processes [12], ion implantation [13], and chemical vapor deposition [9]. Actually, the greatest demand is for nanocomposites in which single domain NPs interact weakly with each other.

The presence of the magnetic properties of the matrix material and/or its special arrangement could lead to the essential modification of both the entire range of properties of the sample and the mechanism of the interparticle interaction. From this viewpoint the CNT matrix is of special interest. Defectless carbon based materials are diamagnetic, while by introducing different kinds of defects and disorder in them, one sees paramagnetic or even ferromagnetic behavior [14–17]. However, in carbon based materials saturation magnetization M_{sat} is not large enough for practical applications of magnetic carbon devices. The M_{sat} value does not usually exceed 0.1 emu g^{-1}, i.e. less than 0.1% of the saturation magnetization of iron. Such magnetism is determined mainly by the peculiar properties of graphene shells which form the CNT walls. Indeed, pure graphene by itself is a diamagnetic material at room temperature, while at low T its intrinsic magnetic properties become paramagnetic [18]. Moreover, embedding point and extended defects [19–21], chemical modification [22–24], and modification of the electronic structure in graphene-based multilayers [25, 26] lead to the emergence of intrinsic room-temperature ferromagnetism in graphene. Therefore, the interaction between magnetic NPs intercalated into the CNT matrix could depend on temperature T, as well as on the CNT defectiveness and NP localization (outside or inside the inner channels of CNTs).

The mechanisms of the interparticle interaction can be studied using different methods. One of the most affordable is the investigation of isothermal magnetic hysteresis loops, $M(H)$. Such magnetostatic parameters like the coercive field H_c, remanence M_{rem}, M_{sat} and their temperature dependencies can be obtained from the $M(H)$ results. Within such an approach it is possible to derive useful information regarding such magnetic properties of the studied materials like magnetization reversal mecahanisms, type of magnetic anisotropy, etc [27–29]. Moreover, the shape of the $M(H)$ curve, in particular, its high field part, could give additional important information about the interparticle interaction. Analyzing the law of the approach to saturation (LAS), it is possible to distinguish the cases of magnetically isolated and strongly interacting via exchange coupling NPs [30–33]. The approach towards saturation is of specific interest for CNT-based nanocomposites with ferromagnetic NPs because this part of the $M(H)$ curve is defined by general characteristics of a sample, and does not contain metastable states [34]. Therefore, the analysis of the LAS for different samples and at various temperatures provides us with a very powerful instrument for the determination of the type of magnetic interparticle interaction [34, 35].

However, the approach developed for the LAS in the past does not take account of possible matrix material contribution, which can significantly vary both the magnetic correlation lengths and the type of coupling between NPs embedded in the magnetic matrix. As was recently demonstrated, even new magnetically ordered states could be induced by peculiarities of interparticle interactions [36, 37].

In this work we have analyzed the LAS for a series of samples of CNT matrix synthesized with low ferromagnetic NP content in the temperature range $T = 2$–350 K, and observed the temperature induced crossover of the mechanisms of the magnetic interaction between NPs. In particular, at low T the coherent magnetic anisotropy determines the extended magnetic order, up to hundreds of nanometers. While close to room temperature, interparticle exchange interaction dominates and the extended magnetic order is lost. When the NP concentration increases, the exchange interaction between them starts to prevail in the entire temperature range studied. The possible mechanisms and the role of the carbon matrix in this crossover are also discussed.

2. Fabrication of samples and experimental details

Floating catalyst chemical vapor deposition (FCCVD) was applied for the synthesis of CNT-based nanocomposites on Si substrates. Ferrocene $Fe(C_5H_5)_2$ was used as a source of catalytic NPs. In this work we studied samples synthesized with a low concentration of ferrocene in ferrocene/xylene solution, $C_F = 0.5$, 0.6, 0.7, 0.8 and 1.0 wt %. The $C_F = 0.5$ wt % corresponds to the lower limit of CNT growth on Si substrate [38]. At such low C_F values catalytic NPs are localized mainly in the inner CNT channels. Starting from $C_F = 1$ wt % they appear outside as well as inside CNT walls [39]. The temperature in the reaction zone was fixed at 1150 K and the growth duration was 1 min. This creates a vertically aligned CNT matrix with a typical thickness of $\approx 20\mu$m. Figures 1(a) and (b) show the scanning electron microscopy (SEM) images, at different magnification, of the cross section of an aligned CNT array synthesized with $C_F = 0.6$ wt %. From figure 1(b) we estimated the average diameter of the CNT as $\varnothing_{CNT} \approx 20$ nm.

In figure 2(a) we show the transmission electron microscopy (TEM) image of a NP intercalated inside a CNT. This sample was synthesized at $C_F = 0.5$ wt %. Using a copper grid covered with a lacey carbon membrane the surface of the glass support containing the carbon nanotubes was scratched a few times. To increase the adhesion between the nanotubes and the carbon membrane (to reduce the vibration during acquisition), after

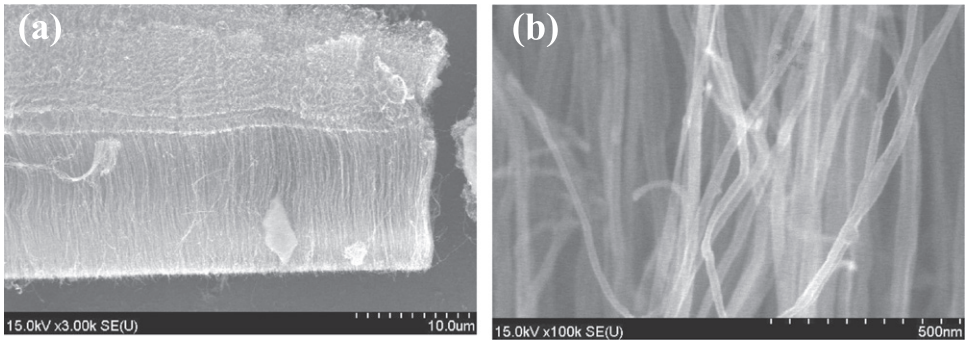

Figure 1. The cross section of the aligned CNT matrix synthesized with $C_F = 0.6$ wt %. (a) The whole cross section, (b) the image of the same sample acquired at higher magnification.

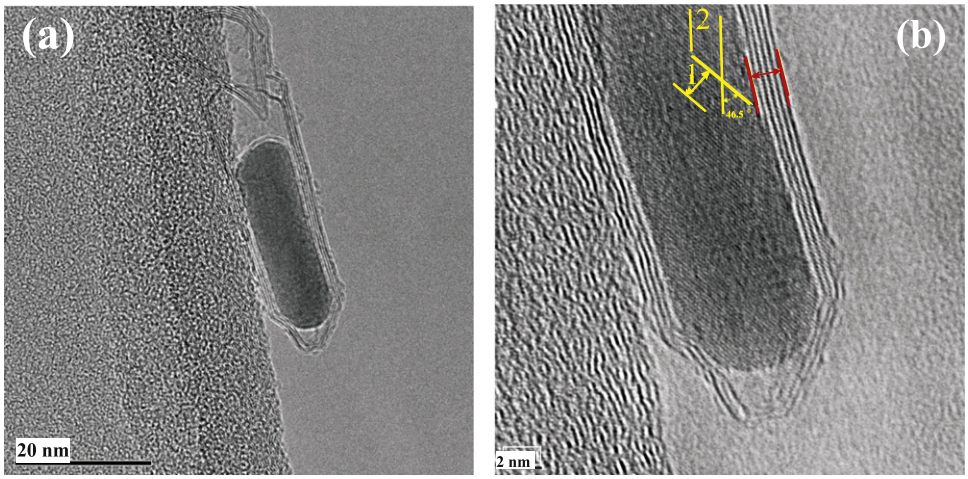

Figure 2. (a) HRTEM image of ferromagnetic nanoparticle intercalated inside CNT, (b) part of the same NP at higher magnification, highlighting two families of planes with distinct orientations (yellow) as well as the carbon shells (red). Sample was synthesized with $C_F = 0.5$ wt %.

the scratching a drop of ethanol was added on the grid, then dried for five minutes under light. To acquire high resolution images a JEOL 2100 microscope with a LaB_6 gun was used. The pixel size was 2004×1334 with an exposure time of 0.5 s. The nanoparticle is observed from the side and it exhibits a clear anisotropic shape of around 5 nm diameter and 25 nm length, thus the aspect ratio is around 5. Figure 2(b) displays the high resolution TEM (HRTEM) image of part of the same particle exhibiting two families of planes with around 5–6 carbon shells on both sides of the NP, which prevents the NP oxidation. The NP is single crystalline all over. The intershell distance of CNTs is 0.34 nm. From the determination of the two distinct interplanar distances and the angle of these two distinct families, it is possible to determine the nature of the nanoparticle, as well as the axis of the particle relative to the graphene shells of the CNT. In the case of figure 2, for example, the NP is clearly iron carbide, ferromagnetic Fe_3C (cementite) with $(1\,\bar{1}\,1)$ orientation along the nanotube axis. A detailed study, however, of the structural properties of such NPs inside CNT inner channels is beyond the scope of the paper and is the topic of a subsequent publication [40], rather than in this one which focuses on the magnetic properties. It is worth mentioning that iron based NPs inserted into CNTs have already been detected [41].

For the sake of clarity, in this article the samples will be named using the number indicating the nominal ferrocene concentration at which the sample was synthesized. For example, the notation 05 is used for the sample synthesized at $C_F = 0.5$ wt % and 10 is used for the sample synthesized at $C_F = 1.0$ wt %.

Figure 3 shows the Raman spectra in 1000–3000 cm^{-1} range recorded with a Nanofinder HE (Lotis-TII) confocal spectrometer. Spectra were acquired with the spectral resolution of 3 cm^{-1} in the backscattering geometry at ambient conditions using a 473 nm wavelength excitation laser. Data refer to samples 05, 06 and 08. All spectra are dominated by two main bands, G ($\approx$1580 cm^{-1}) and D ($\approx$1357 cm^{-1}) and have been normalized to the amplitude of D peak for each sample. The G band is broadened, which is characteristic of CNTs [42]. The D band corresponds to the ruinous hexagonal lattice of graphitic carbon. The first overtone of the D band (2D

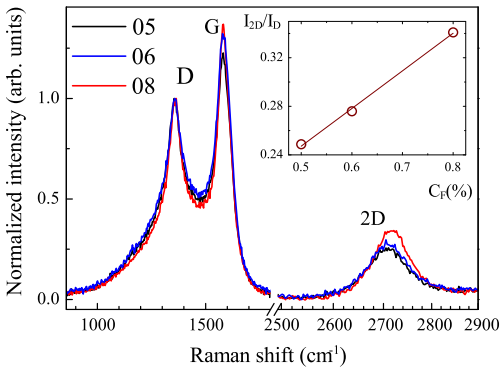

Figure 3. Normalized Raman spectra of samples 05, 06, and 08. Inset: 2D/D ratio intensity versus the ferrocene concentration (symbols). Line corresponds to the result of the linear best fit procedure.

band) is usually found at ≈2715 cm^{-1}, is always present for CNT Raman spectra and its intensity tends to increase with graphitization [43]. Moreover, as it has been shown recently, carbon defects are clearly manifested by analyzing the ratio of intensitiy I_{2D}/I_D [44]. It has been demonstrated that the 2D/D ratio intensity is increased with the decrease in the defectiveness of carbon which occurs when the nanotube diameter increases [44, 45]. In the inset of figure 3 we show the 2D/D ratio intensity versus the ferocene concentration. The linear increase of I_{2D}/I_D with C_F can be clearly seen, which could be reasonably associated with improvement in the quality of carbon structure.

Magnetic properties were studied by measuring isothermal magnetic hysteresis loops, $M(H)$, in the temperature range 2–350 K. For that we used a SQUID magnetometer (Quantum Design). The magnetic field was always oriented parallel to the CNT axis (i.e. perpendicular to the surface substrate) and varied in the range from −5 to +5 T. The magnetic moment was measured with the sensitivity of 10^{-6} emu. Samples were mounted inside a nonmagnetic tube and were fixed by two straws creating some backlash, which was a little different for the various samples. This lack of material created a linear with respect to the magnetic field signal, which was independent of temperature and slightly varied from sample to sample.

Finally, the main ferromagnetic phase of catalytic NPs for low C_F samples is α-Fe with M_{sat} and Curie temperature, T_C, values easily less than for bulk iron [46]. Also some small amount of iron carbide phases like cementite Fe_3C, Hagg phase Fe_5C_2, Fe_7C_3 could be present in our samples [40]. For $C_F > 1$ wt % the cementite phase becomes dominant [46]. More details about sample fabrication and characterization can be found elsewhere for $C_F > 1$ wt% [39, 46, 47] and $C_F < 1$ wt % [39].

3. Results

The magnetization curves measured at $T = 2$ K for different samples are presented in figure 4. The magnetization values are normalized to the M value at $H = 20$ kOe. The evolution of the symmetric magnetic hysteresis loops shows a widening tendency towards the higher C_F concentrations. Similar results were obtained for all other temperatures. The observed paramagnetic-like behavior in the saturation part of the $M(H)$ loops was caused by the discontinuity of the sample holder [48]. This signal, measured at $T = 100$ K without sample, is shown in figure 4 by the solid line.

In figure 5 we present the upper part of the $M(H)$ loops measured for sample 08 in the temperature range 2–350 K after subtracting the linear response of the sample holder. These data were used for the analysis of the magnetization in the approach to saturation ($H > 1$ kOe).

Analysis of the LAS provides important information regarding the mechanisms of the interparticle interaction and correlation in the orientation of the magnetic anisotropy axes of NPs in real space [49]. In the limiting cases, the LAS is expressed as [50]

$$\frac{\delta M}{M_{sat}} = \frac{M_{sat} - M(H)}{M_{sat}} \sim H^{-s}, \quad (1)$$

where the exponent s depends on the relation between H and the exchange field H_{ex}. For $H \ll H_{ex}$ in the case of a three-dimensional (3D) nanocomposite the exponent is $s = 1/2$. This corresponds to the dominant role of the exchange coupling, while for $H \gg H_{ex}$ NPs are not interacting, the magnetic anisotropy is the main mechanism and $s = 2$ (0 dimensionality) [34]. Moreover, if there is some particular arrangement of the NPs, in the limit $H \ll H_{ex}$, the exponent s can be equal to 1 (2D nanocomposite) or 3/2 (1D nanocomposite) [50].

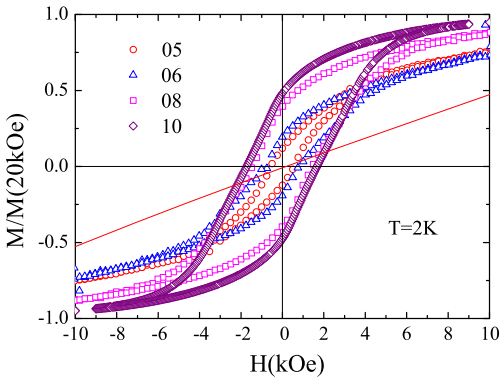

Figure 4. Field dependence of the normalized magnetization $M/M(20\,\text{kOe})$ for samples 05, 06, 08 and 10 at $T = 2$ K (symbols). The solid line corresponds to the normalized linear response of the sample holder measured at $T = 100$ K.

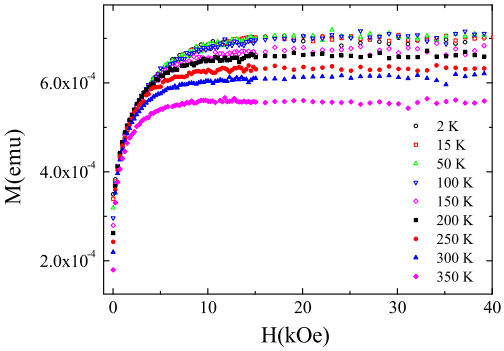

Figure 5. The upper part of the $M(H)$ loops for sample 08 measured at different temperatures and after subtracting the linear response of the sample holder.

Consequently, there is a perception that the analysis of the exponent s in the law (1) allows us to set the dimensionality of the magnetic nanocomposite [50]. Therefore we first try to apply this approach to the analysis of our data. In figure 6 we plot the high field part of the magnetization curves, according to equation (1), for sample 08. In particular, in figure 6(a) we plot $\delta M/M_{\text{sat}}$ versus H^{-2}, in the figure 6(b) $\delta M/M_{\text{sat}}$ versus $H^{-3/2}$ is shown, in figure 6(c) we plot $\delta M/M_{\text{sat}}$ versus H^{-1} and, finally, in figure 6(d) $\delta M/M_{\text{sat}}$ versus $H^{-1/2}$ is depicted. All data in figure 6 are for three temperatures, $T = 2$, 150, and 300 K. For the sake of convenience, on the upper horizontal axes we plot the absolute values of the magnetic field.

At first glance, the exponent s in the LAS (1) cannot be determined unambiguously. Indeed, the main result followed from figure 6 is that at each temperature it is possible to find a certain interval of the magnetic field, in which one or another exponent s is valid. We try to clarify the situation by analyzing the width of the magnetic field range, ΔH_s, where the LAS (1) is valid, for each s value and each temperature T. This result for the sample 08 is presented in figure 7. From the data of figure 7 it follows that the ΔH_s values vary significantly with the exponent s and temperature. In particular, for the temperature interval $2 - 100$ K the widest range of ΔH_s corresponds to $s = 2$. For high temperatures, $200\ K < T < 350$ K, the exponent $s = 1/2$ gives the agreement with the experiment in the widest magnetic field range. At that interval ΔH_s for all other exponents are absorbed by the dominant interval. Finally, for the intermediate temperatures, $T = 100$ and 150 K, the ΔH_s values for $s = 2$, 3/2 or 1 are practically the same and for $T = 200$ K it is impossible to distinguish the cases of $s = 2$ and 1/2.

Data presented in figures 6(a)–(d) and 7 are typical for samples 05, 06, 07 and 08. We attribute a wider range of validity of the LAS (1) for a given exponent with a dominant dimensionality which is determined by this exponent. It means that for low C_F samples (i.e. low content of ferromagnetic NPs localized inside CNT channels) the dimensionality of the nanocomposite changes from mainly 0D at low T to mainly 3D at high T via the mixed status at which different dimensionalities are realized simultaneously.

The value of the exponent s as well as its temperature behavior for sample 10 significantly differ. The dimensionality of this nanocomposite does not depend on temperature and is equal to 3D (i.e. $s = 1/2$). In figure 8 we show the $\delta M/M_{\text{sat}}$ versus $H^{-1/2}$ for this sample at three temperatures, $T = 2$, 150 and 300 K. Again, for the sake of convenience, on the upper horizontal axis we plot the absolute values of the magnetic field. It is clearly

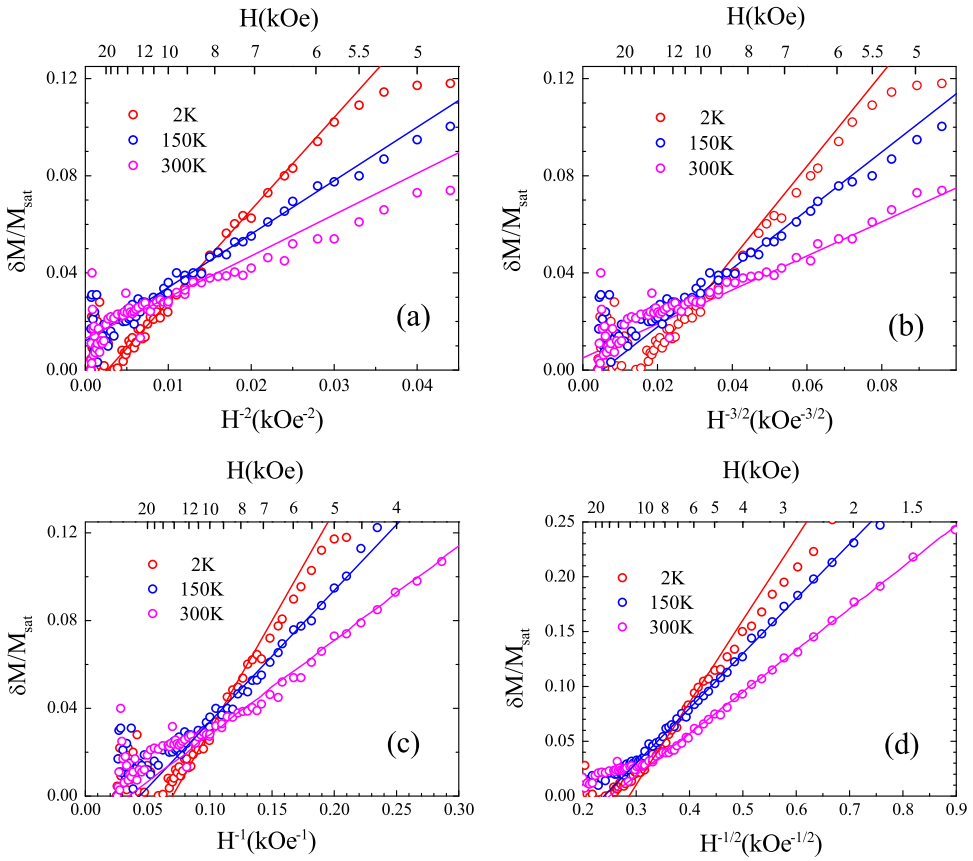

Figure 6. Analysis of LAS according to equation (1) for sample 08 and different exponent s values. Symbols are for the experimental data, lines are for the result of the best fit procedure. The range of the magnetic field in which the LAS is studied can be estimated from the upper horizontal axis. Data are for $T = 2$, 150 and 300 K. (a) $s = 2$, (b) $s = 3/2$, (c) $s = 1$, (d) $s = 1/2$.

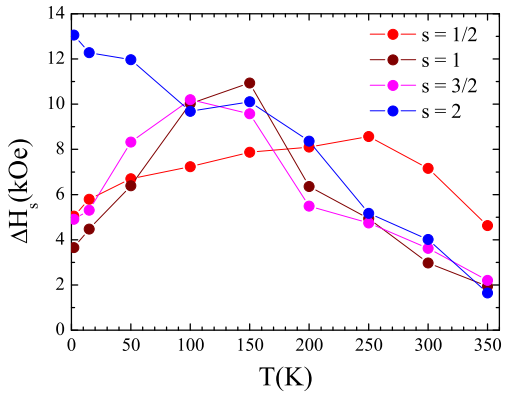

Figure 7. Temperature dependence of ΔH_s for the sample 08 for different exponents s from equation (1).

seen that for $T = 2$ K the exponent $s = 1/2$ is valid in the magnetic field range 4 – 10 kOe and for $T = 300$ K this interval is 2.5 – 6.5 kOe. In the upper left inset to the figure 8 we show the temperature dependence of ΔH_s for $s = 1/2$. This exponent value gives the maximum interval for the LAS (1) in the entire temperature range studied . In other words, the exponent s for sample 10 is temperature independent and is equal to 1/2. This is in agreement with our previous result concerning samples with $C_F = 1$ and 10 wt % [46]. In the lower right inset to the figure 8 we show the data $\delta M/M_{sat}$ for this sample plotted versus H^{-2}. The scale of the magnetic field is close to that of the main plot and the linear portion in the substantial field interval cannot be found on this dependence.

The unequivocal message from the analysis performed is that for samples synthesized with low C_F content ($C_F < 1$ wt%) the *qualitative change* of LAS with temperature does exist. The $\delta M/M_{sat}$ versus H dependencies vary from H^{-2} at low T to $H^{-1/2}$ at high T, subsequently crossing out all possible values of s. However, for samples

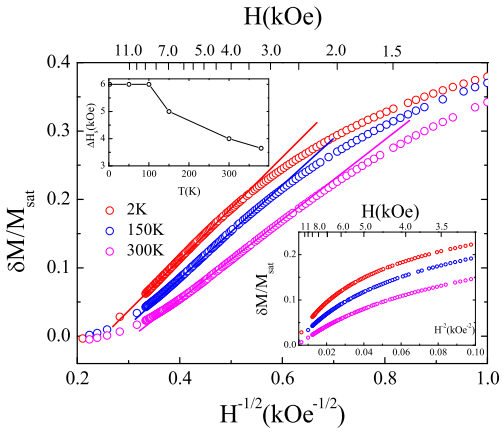

Figure 8. Analysis of LAS according to equation (1) for sample 10. Symbols are for the experimental data, lines are for the result of the best fit procedure. Data are for $T = 2$, 150 and 300 K. The main plot corresponds to the exponent $s = 1/2$. The range of the magnetic field in which the LAS is studied can be estimated from the upper horizontal axis. Upper left inset: temperature dependence of the ΔH_s for $s = 1/2$. Lower right inset: analysis of LAS according to equation (1) for sample 10 and for the exponent $s = 2$. Symbols are for the same experimental data as in the main plot. The range of the magnetic field in which the LAS is studied can be estimated from the upper horizontal axis.

synthesized with high C_F values, $C_F \geqslant 1$ wt %, the exponent s is temperature independent and is equal to 1/2. This is the main result of the experimental data elaboration which will be discussed in detail in the following section.

4. Discussion

We use standard theoretical models for the quantitative analysis of the experimental data such as the random anisotropy model (RAM) [35, 46, 51–53] and the LAS [34, 46, 50, 54–57]. Both these approaches are widely exploited for the analysis of the magnetic properties of amorphous and polycrystalline ferromagnets.

One of the key parameters characterizing the magnetic properties of the nanocomposite are the local random anisotropy field H_{ra} and the exchange field H_{ex}. Within the RAM they are expressed as

$$H_{\mathrm{ra}} = \frac{2\,K}{M_{\mathrm{sat}}} \tag{2}$$

and

$$H_{\mathrm{ex}} = \frac{2A}{M_{\mathrm{sat}} R_a^2}, \tag{3}$$

respectively. In equations (2) and (3) the constant K is the effective magnetic anisotropy, A is the constant of the exchange coupling, R_a is the length over which the magnetic anisotropy axes are correlated. Usually in a nanocrystalline material R_{a} is assumed to be equal to the radius of the nanoparticle [50, 57].

The values of H_{ra} and H_{ex} were evaluated according to the algorithm evolved earlier in [46]. In particular, the saturation magnetization was taken from [46] as $M_{\mathrm{sat}} = (1.26 - 1.33) \times 10^5$ A m^{-1}. R_{a} was assumed to be equal to half of the average diameter of CNT, $R_{\mathrm{a}} \approx \varnothing_{\mathrm{CNT}}/2 \approx 10$ nm. Finally, A was calculated as $A = (3 - 5) \times 10^{-12}$ J m^{-1} [46]. As a result, we get, depending on the sample and temperature, $H_{\mathrm{ra}} = 3$–6 kOe, $H_{\mathrm{ex}} = 2$–5 kOe. These estimations imply that the values of the exchange field fall within, or are very close to, the range of the LAS. It means that well known simple models for the LAS, strictly speaking, cannot be applied for the quantitative experimental data interpretation, because they have asymptotic character, i.e. are valid only in the limits $H \ll H_{\mathrm{ex}}$ and $H \gg H_{\mathrm{ex}}$ [35, 49].

In our case it is necessary to apply the approach, which operates for the intermediate fields $H \sim H_{\mathrm{ex}}$ [34, 49]. Generally, along with the exchange interaction both local *random* and *coherent* anisotropies should be considered [53]. In this case, the expression for the density of the magnetic energy of the system can be written as [53]

$$\epsilon = \frac{1}{2} A\,(\nabla \cdot \mathbf{M})^2 - \frac{1}{2}\beta_{\mathrm{ra}}\,(\mathbf{M} \cdot \mathbf{n})^2 - \mathbf{H}\cdot\mathbf{M} - \frac{1}{2}\beta_{\mathrm{ca}}\,(\mathbf{M} \cdot \mathbf{N})^2, \tag{4}$$

where the magnetization **M** is assumed to be of the fixed length M_{sat}, **n** is a unit vector of the random anisotropy, **N** is a unit vector of the coherent anisotropy, constants β_{ra} and β_{ca} are a measure of the local random anisotropy (LRA) and coherent anisotropy (CA), correspondingly. Here the uniaxial NPs are assumed and vector **N** does not vary. Constants β_{ra} and β_{ca} are proportional to H_{ra} and the coherent anisotropy field H_{ca}, respectively. The spatial variations of the anisotropy field are characterized by a correlation function $C(x)$ which obeys the law

$$C(0) = 1,\ C\left(x \gg R_a\right) \to 0, \tag{5}$$

where x is a coordinate.

The magnetization law for the whole region of approaching saturation, neglecting the CA, is [34]

$$\frac{\delta M(H)}{M_{sat}} = \frac{K^2 R_H}{30A^2}\int_0^\infty \mathrm{d}^3x\ \exp\left(-x/R_H\right)x^2C(x), \tag{6}$$

where $R_H = (A/M_{sat}H)^{1/2}$. Thus, the short range correlation function can be extracted analyzing $\delta M(H)$ by applying the inverse Laplace transformation. Equation (6) can be rewritten as

$$\frac{\delta M(H)}{M_{sat}} = \frac{\lambda^2}{30p(H)}\int_0^\infty \mathrm{d}^3r\ \exp\left[-p(H)r\right]r^2C(r) \tag{7}$$

with $p(H) = \sqrt{H/H_{ex}}$, $r = x/R_a$, $\lambda = H_{ra}/H_{ex}$.

Additional consideration of the CA leads to a change to equation (7). Indeed, as was first discussed in [53], taking account of the CA results in the modification of the LAS. In particular, such auxiliary quantities like the coherent anisotropy correlation length $\delta_{ca} \sim R_a(H_{ex}/H_{ca})^{1/2}$ and field $H_{sa} \equiv H_{ra}^4/H_{ex}^3$ are introduced in the theory. The latter is strongly related to the angle $\Theta \sim (H_{sa}/H)^{1/4}$ over which magnetic moments tip from the magnetic field direction. The field of the coherent anisotropy can be evaluated from the correlation function. In the presence of a field $H > H_{ca}$ in equation (7) one needs to simply replace H by $H + H_{ca}$ [53]. Thus, the final expression for the LAS in the presence of both LRA and CA contributions is

$$\frac{\delta M(H)}{M_{sat}} = \frac{\lambda^2}{30p\left(H + H_{ca}\right)}\int_0^\infty \mathrm{d}^3r\ \exp\left[-p\left(H + H_{ca}\right)r\right]r^2C(r). \tag{8}$$

Hereinafter we will use equation (8) for the fitting procedure and $C(r)$ determination. First we will discuss data related to the samples 05, 06, 07 and 08.

The analysis performed revealed that, for the best fit procedure of the experimental data the value of the Laplace integral $F(p) = \int_0^\infty 4\pi\ \exp(-pr)r^2C(r)\,\mathrm{d}r$ in the temperature range 2–200 K is close to p^{-3}. It means that using the boundary conditions (5) the correlation function is the Fermi–Dirac-like

$$C_1(r) = \frac{1}{1 + \exp\left(\frac{r - r_{1/2}}{2}\right)}, \tag{9}$$

where $r_{1/2}$ is a coordinate at which the value of the correlation function is equal to 1/2. This correlation function is shown in figure 9 by the solid line.

However, in the high temperature range, $T > 200$ K, the Laplace integral was obtained as $F(p) = G\exp(-b/p)p^{-\nu-1}$, where G, b and ν are constants. For such Laplace representation the correlation function is

$$C_2(r) = b^{-1/2}r^{(\nu/2)-2}J_\nu\left[2b^{1/2}\left(r + r_0\right)^{1/2}\right], \tag{10}$$

where J_ν is the νth order Bessel function of the first kind and r_0 is a constant. This correlation function is shown in figure 9 by the dashed line. Note that for the above considered Laplace integrals the analytical expression for the LAS does not exist.

In the intermediate temperature interval ($T = 100$–200 K) the experimental data can also be fitted with the Laplace integrals $F(p) \approx p^{-1}$ and $F(p) \approx p^{-2}$. The first Laplace integral leads to the correlation function

$$C_3(r) = \frac{1}{r^2}, \tag{11}$$

while the second one gives

$$C_4(r) = \frac{1}{r}. \tag{12}$$

Note that equations (11) and (12) are valid for $r > 1$, while for $0 \leqslant r \leqslant 1$ it was assumed $C_3(r) = C_4(r) = 1$. It should also be noted that the correlation function $C_3(r)$ leads to the exponent $s = 1$ and $C_4(r)$ corresponds to the exponent $s = 3/2$ in the LAS (1).

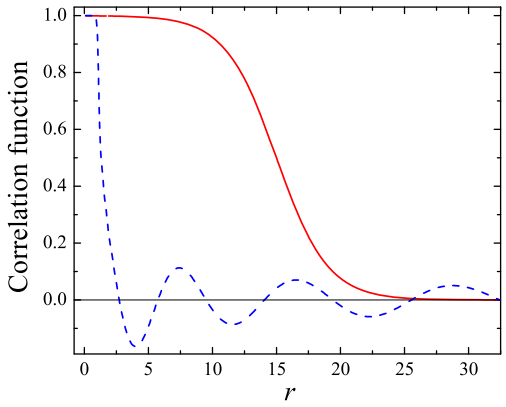

Figure 9. Correlation functions for sample 08 according to equation (9), $C_1(r)$, (solid line, temperature range 2–200 K) and equation (10), $C_2(r)$, (dashed line, temperature range 200–350 K).

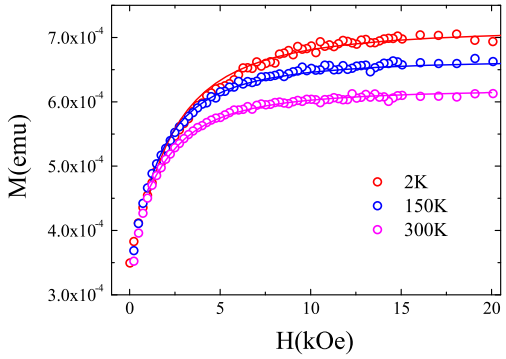

Figure 10. Analysis of LAS for sample 08 at different temperatures. Symbols are for the experiment, solid lines refer to the best fit procedure according to equation (8). For $T = 2$ and 150 K the correlation function was $C_1(r)$, while for $T = 300$ K the correlation function $C_2(r)$ resulted in the best agreement with the experiment.

Consequently, applying the boundary conditions (5), the following general analytical expression is valid for the LAS in the cases $s = 1$ and 3/2

$$\frac{\delta M}{M_{sat}} = \frac{4\pi}{15}\left(\frac{H_{ra}}{H + H_{ca}}\right)^2\left[1 - exp\left(-\frac{H + H_{ca}}{H_{ex}}\right)^{1/2}\right]\left[1 + n \times \left(\frac{H + H_{ca}}{H_{ex}}\right)^{1/2}\right], \quad (13)$$

where for $s = 1$, the multiplier $n = 1$, and for the exponent $s = 3/2$ we got $n = 1/2$.

The results of the fitting procedure according to equation (8) with the correlation functions $C_1(r)$ ($T < 200$ K) and $C_2(r)$ ($T > 200$ K) for sample 08 are shown in figure 10.

It can clearly be seen from figure 10 that now the theory explains well the wider range of the experimental data, from $H = 1$ kOe up to saturation. The range of the agreement between theory and experiment (≈20 kOe) is much greater than ΔH_s values obtained before (see figure 7) assuming for the LAS the simple expression (1). At this point we would also like to emphasize that the fit of the experimental data according to equation (7), i.e. excluding the mechanism of the coherent anisotropy, was impossible.

The exhaustive analysis of the experimental data offered us the possibility of estimating such important parameters of the CNT matrix with low ferromagnetic NP content, like H_{ex}, H_{ra} and H_{ca} and of analyzing their temperature dependencies. These values for sample 08 are summarized in table 1.

From the results shown in table 1 it follows that the values of H_{ca} are indeed very high for $T < 200$ K. The asterisk in numbers means that for these H_{ca} the quantity $r_{1/2} = 5$, while for low T this value is $r_{1/2} = 15$, in agreement with figure 9. Another important result which follows from table 1 is the presence of the coherent anisotropy even at high T, where the correlation function is Bessel and the exchange interaction dominates. But the value of H_{ca} becomes very low, less than 1 kOe. Finally, it should be mentioned that for $C_1(r)$ the best fit results were insensitive to the H_{ex} values in the interval from 4 to 8 kOe.

The results for sample 08 presented in table 1 are typical for samples 05, 06, 07 and 08.

Table 1. Values of H_{ex}, H_{ra} and H_{ca} (all in kOe) at different temperatures T as obtained from the fitting procedure for sample 08 and different correlation functions. $C_1(r)$, $C_2(r)$, $C_3(r)$ and $C_4(r)$ are expressed by equations (9)–(12), respectively. Temperature T is in Kelvin.

	$C_1(r)$			$C_2(r)$			$C_3(r)$			$C_4(r)$		
T	H_{ex}	H_{ra}	H_{ca}	H_{ex}	H_{ra}	H_{ca}	H_{ex}	H_{ra}	H_{ca}	H_{ex}	H_{ra}	H_{ca}
2	4.0	3.1	3.5	4.0	4.0	1.6	2.0	3.5	2.0	2.0	3.2	2.5
15	4.0	3.1	3.5	4.0	4.0	1.6	2.0	3.5	2.0	2.0	3.2	2.5
50	4.0	3.1	3.5	4.0	4.0	1.6	2.0	3.5	2.0	3.0	3.5	2.5
100	4.0	3.1	3.5	4.0	3.9	1.5	2.0	3.5	2.0	3.0	3.5	2.5
150	4.0	3.0	3.5	4.0	3.4	1.0	3.0	3.5	2.0	3.0	2.8	1.8
200	4.0	3.0*	3.2*	3.0	2.7	1.0	3.0	3.5	2.0	4.0	2.6	1.5
250	4.0	3.0*	3.2*	3.0	2.5	0.8	4.0	3.5	1.8	4.0	2.5	1.5
300	4.0	2.7*	2.9*	3.0	2.5	0.8	4.0	3.5	1.8	4.0	2.5	1.5
350	4.0	2.0*	2.0*	3.0	2.2	0.8	4.0	3.5	1.8	5.0	2.5	1.0

On the basis of the obtained parameters it is possible to estimate the coherent anisotropy correlation length and angle Θ over which magnetic moments deviate from the field direction. Estimations reveal that H_{sa} varies in the range from 1.4 kOe, for sample 08, to 4.8 kOe, for sample 05, which corresponds to the angle $\Theta = 45°$ and 59°, correspondingly. At these, δ_{ca} practically does not vary from sample to sample and is almost equal to the length of the correlation of the magnetic anisotropy axes R_a, i.e. $\delta_{ca} \approx R_a$. All these estimations were done for $T = 2$ K.

However, from the obtained $C_1(r)$ it follows that at low temperatures the coherence is extended over much greater distances, up to $x_{1/2} \approx r_{1/2}R_a \approx 100-150$ nm, see solid line in figure 9. It is worth mentioning that the distance 150 nm is an upper limit of the interparticle spacing usually observed by TEM inside CNTs synthesized at low C_F content [58].

Such discrepancy (one order of magnitude) between the $x_{1/2}$ values obtained from the correlation function and the δ_{ca} values estimated from the considerations described in [53] could be due to the following reasons. Usually it is assumed to be the exponential decay of the coherence in magnetic nanocomposites. Then it is natural to get $\delta_{ca} \approx x_{1/2} \approx R_a$. But in our case it is not. We believe that the extended coherence in our samples with magnetic NPs localized mainly inside CNTs is due to the influence of the carbon medium. Indeed, when magnetic NPs are intercalated inside inner channels of CNTs, they can interact with each other via such magnetic media as a carbon nanotube. The exact mechanism of this interaction is still unclear, but it is reasonable to suppose that, even though the magnetism of a carbon based medium is weak, it could occur via, e.g., the indirect exchange coupling, stimulating the propagation of the extended magnetic order in our samples. It is worth mentioning also that the defectiveness of CNTs (see figure 3) could stimulate the magnetic order in them. The alignment of CNTs is also important in this case. As we showed recently, the destruction of the alignment leads to the loss of the extended order [46, 59].

With increasing temperature the extended magnetic order is also lost. This shows that thermal energy is important, as well as the reduction in the H_{ca} values (see table 1). The latter could reflect the possible weakening of the CNT magnetic properties with temperature. The significant reduction in H_{ca} values could also lead to the violation of the inequality $(H + H_{ca}) \gg H_{ex}$ which, in turn, makes the observation of the exponent $s = 2$ difficult and strengthens the exchange coupling.

For sample 10 the magnetization curves are described by equation (8) for the whole temperature range *only* when using the $C_2(r)$ correlation function (equation (10)). The result of the fitting procedure is shown in figure 11. Note that during this fit the field of the coherent anisotropy was exactly equal to zero.

The weak oscillating character of the obtained Bessel correlation functions does not mean, in our opinion, the oscillation of the magnetic anisotropy. We believe it could be mostly caused by the peculiarities in the exchange interparticle interaction and the influence of the CNT matrix on it. Indeed, the indirect exchange coupling characterizes the carbon nanotubes [60]. This could cause the oscillating character of the exchange coupling, which is reflected in the weakening and strengthening of the magnetic anisotropy contribution along the CNT. But this mechanism is absent in the model which has been applied to the discussion of the experimental data.

5. Conclusions

The magnetic properties of a CNT matrix synthesized by FCCVD with low C_F concentrations have been investigated in a wide temperature range, from $T = 2$ K to $T = 350$ K. It has been demonstrated that studying approaching saturation is a very powerful method for determining the mechanisms of interparticle interaction.

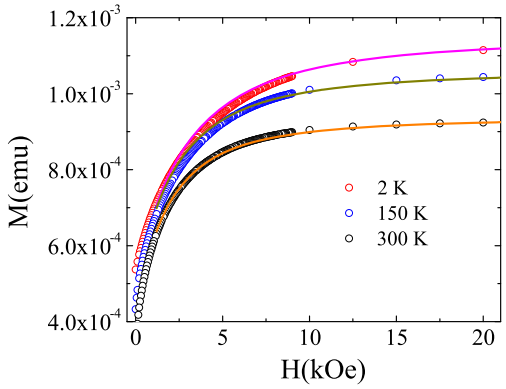

Figure 11. Analysis of LAS for sample 10 at different temperatures. Symbols are for the experiment, solid lines refer to the best fit procedure according to equation (8). For all temperatures $C_2(r)$ was applied (equation (10)).

For samples synthesized with $C_F < 1$ wt % the coherent anisotropy dominates at $T < 200$ K. At this temperature the H_{ca} values are almost comparable or even exceed the exchange field H_{ex}. The correlation length of the coherent magnetic anisotropy is macroscopically large and is extended up to 150 nm. This is caused by a special arrangement of NPs inside the CNTs and, probably, by the inner magnetism of the CNTs. The observed extended magnetic order could be important for new spintronic devices.

At $T > 200$ K this coherence is lost because of the reduction in the H_{ca} values. As a result, the exchange coupling becomes dominant. The dimensionality of the nanocomposite becomes 3D. This crossover, from 0D at low T to 3D at high temperatures occurs via other possible values of dimensionality, namely 1D and 2D.

For samples synthesized with $C_F = 1$ wt % the exchange coupling always dominates in the entire temperature range studied. Nevertheless, the possible inner magnetic properties of CNTs manifest in the Bessel-like correlation function of the magnetic anisotropy axes, which could reflect the presence of the indirect exchange coupling via the carbon medium. More work is in progress now to clarify the role of the carbon medium and the alignment of NPs on the interparticle interaction.

Acknowledgments

This work was partially supported by the Belarusian Foundation for Basic Research, grant no. F13F-002 (ALD, IVK, SLP) and by the FP-7 Programme, grant agreement no. 295016 (BELERA) (ALD, IVK, VAL, FLN, SLP). G Melinte and C Speisser are acknowledged for TEM measurements and analysis. The work of JMH JT has been supported by Spanish Government Project No. MAT2011-23698.

References

[1] Liu K, Nagodawithana K, Searson P and Chien C 1995 *Phys. Rev.* B **51** 7381
[2] Tsoi M, Sun J, Rooks M, Koch R and Parkin S 2004 *Phys. Rev.* B **69** 100406(R)
[3] Mehta K K, Wu T-H and Chiou E P Y 2008 *Appl. Phys. Lett.* **93** 254102
[4] Gao N, Wang H J and Yang E H 2010 *Nanotechnology* **21** 105107
[5] Choi D S *et al* 2008 *J. Nanosci. Nanotechnol.* **8** 2323
[6] Faupel F, Zaporojtchenko V, Strunkus T and Elbahri M 2010 *Adv. Eng. Mater.* **21** 1177
[7] Laurent S, Forge D, Port M, Roch A, Robic C, Els L V and Müller R N 2008 *Chem. Rev.* **108** 2064
[8] Granitzer P and Rumpf K 2011 *Materials* **4** 908
[9] Jourdain V and Bichara C 2013 *Carbon* **58** 2
[10] Liu J, Qiao S Z, Hu Q H and (Max) Lu G Q 2011 *Small* **7** 425
[11] Tarasenka N, Butsen A, Pankov V and Tarasenko N 2013 *Phys. Status Solidi* B **250** 809
[12] Dolgiy A, Redko S V, Bandarenka H, Prischepa S L, Yanushkevich K, Nenzi P, Balucani M and Bondarenko V 2012 *J. Electrochem. Soc.* **159** D623
[13] Orléans C D, Stoquert J P, Estournès C, Cerruti C, Grob J J, Guille J L, Haas F, Muller D and Richard-Plouet M 2003 *Phys. Rev.* B **67** 220101(R)
[14] Esquinazi P and Höhne R 2005 *J. Magn. Magn. Mater.* **290-291** 20
[15] Yang X, Xia H, Qin X, Li W, Dai Y, Liu X, Zhao M, Xia Y, Yan S and Wang B 2009 *Carbon* **47** 1399
[16] Rode A V, Gamaly E G, Christy A G, Fitz Gerald J G, Hyde S T, Elliman R G, Luther-Davies B, Veinger A I, Androulakis J and Giapintzakis J 2004 *Phys. Rev.* B **70** 054407
[17] Akhurov M A, Katsnelson M I and Fasolino A 2013 *J. Phys.: Condens. Matter* **25** 255301
[18] Sepioni M, Nair R R, Rablen S, Narayanan J, Tuna F, Winpenny R, Geim A K and Grigorieva I V 2010 *Phys. Rev. Lett.* **105** 207205
[19] Červenka J, Katsnelson M I and Flipse C F J 2009 *Nat. Phys.* **5** 840

[20] Yazev O V 2010 *Rep. Prog. Phys.* **73** 056501
[21] Santos E J G, Ayuela A and Sánchez-Portal D 2012 *New J. Phys.* **14** 043022
[22] Son Y-W, Cohen M L and Louie S G 2006 *Nature (London)* **444** 347
[23] Lehtinen P O, Foster A S, Ayuela A, Krasheninnikov A, Nordlung K and Nieminen R M 2003 *Phys. Rev. Lett.* **91** 017202
[24] Giesbers A J M, Uhlirová K, Konečny M, Peters E C, Burghard M, Aarts J and Flipse C F J 2013 *Phys. Rev. Lett.* **111** 166101
[25] Castro E V, Peres N M R, Stauber T and Silva N A P 2008 *Phys. Rev. Lett.* **100** 186803
[26] Pisani L, Montanari B and Harrison N M 2008 *New J. Phys.* **10** 033002
[27] Dormann J L, Fiorani D and Tronc E 1997 *Adv. Chem. Phys.* **98** 283
[28] Varvaro G, Albertini F, Agostinelli E, Casoli F, Fiorani D, Laureti S, Lupo P, Ranzieri P, Astinchap B and Testa A M 2012 *New J. Phys.* **14** 073008
[29] Navas D *et al* 2012 *New J. Phys.* **14** 113001
[30] Akulov N S 1931 *Ztschr. Physik* **67** 794
[31] Brown W T Jr 1940 *Phys. Rev.* **58** 736
[32] Fahnle M and Kronmuller H 1978 *J. Magn. Mag. Mater.* **8** 149
[33] Chudnovsky E M and Serota R A 1983 *J. Phys.* C **16** 4181
[34] Chudnovsky E M 1989 *J. Magn. Magn. Mater.* **79** 127
[35] Chudnovsky E M 1988 *J. Appl. Phys.* **64** 5770
[36] Martínez-Huerta J M, de la Torre Medina J, Piraux L and Encinas A 2013 *J. Phys.: Condens. Matter* **25** 226003
[37] Hiroi K, Kura H, Ogawa T, Takahashi M and Sato M 2014 *J. Phys.: Condens. Matter* **26** 176001
[38] Kumar M and Ando Y 2010 *J. Nanosci. Nanotechn.* **10** 3739
[39] Labunov V, Prudnikava A, Yanushkevich K, Basaev A, Danilyuk A, Yu Fedotova and Shulitskii B 2011 *Carbon nanotubes: applications on electronic devices* ed J M Marulanda (InTech 71)
[40] Speisser C, le Normand F, Melinte G, Ersen O, Komissarov I V, Labunov V A and Prischepa S L in preparation
[41] Blank V D, Gorlova I D, Hutchison J L, Kiselev N A, Ormont A B, Polyakov E V, Sloan J, Zakharov D N and Zybtsev S G 2000 *Carbon* **38** 1217
[42] Rao A M, Jorio A, Pimenta M A, Dantas M S S, Saito R, Dresselhaus G and Dresselhaus M S 2000 *Phys. Rev. Lett.* **84** 1820
[43] Wang Y, Alsmeyer D C and mc Creery R L 1990 *Chem Mater* **2** 557
[44] Bokova S N, Obraztsova E D, Grebenyukov V V, Elumeeva K V, Ishchenko A V and Kuznetsov V L 2010 *Phys. Status Solidi* B **247** 2827
[45] Tessonnier J-P *et al* 2009 *Carbon* **47** 1779
[46] Danilyuk A L, Prudnikava A L, Komissarov I V, Yanushkevich K I, Derory A, Le Normand F, Labunov V A and Prischepa S L 2014 *Carbon* **68** 337
[47] Labunov V A, Shulitski B G, Prudnikava A L and Yanushkevich K I 2008 *J. Phys.: Conf. Ser.* **100** 052095
[48] Sawicki M, Stefanowicz W and Ney A 2011 *Semicond. Sci. Technol.* **26** 064006
[49] Chudnovsky Eugene M 1995 The Magnetism of Amorphous Metals and Alloys ed J A Fernandez-Baca and Wai-Yim Ching (World Scientific Singapore) Chap. 3
[50] Iskhakov R S, Komogortsev S V, Balaev A D and Chekanova L A 2000 *Pis. Zh. Eksp. Teor. Fiz.* **72** 440
Iskhakov R S, Komogortsev S V, Balaev A D and Chekanova L A 2000 *JETP Lett.* **72** 304 (Engl. transl.)
[51] Harris R, Plischke M and Zuckerman M J 1973 *Phys. Rev. Lett.* **31** 160
[52] Alben R, Becker J J and Chi M C 1978 *J. Appl. Phys.* **49** 1653
[53] Chudnovsky E M, Saslow W M and Serota R A 1986 *Phys. Rev.* B **33** 251
[54] Ignatchenko V A, Iskhakov R S and Popov G V 1982 *Zh. Eksp. Teor. Fiz.* **82** 1518
Ignatchenko V A, Iskhakov R S and Popov G V 1982 *Sov. Phys. JETP* **55** 878 (Engl. transl.)
[55] Tejada J, Martinez B, Labarta A, Grössinger R, Sassik H, Vazguez M and Hernando A 1990 *Phys. Rev.* B **42** 898
[56] Chudnovsky E M and Tejada J 1993 *Europhys. Lett.* **23** 517
[57] Löffler J F, Meier J P, Doudin B, Ansermet J-P and Wagner W 1998 *Phys. Rev.* B **57** 2915
[58] Le Normand F *private communication*
[59] Prischepa S L, Danilyuk A L, Prudnikava A L, Komissarov I V, Labunov V A and Le Normand F 2014 *Phys. Status Solidi* C **11** 1074
[60] Costa A T Jr, Kirwan D F and Ferreira M S 2005 *Phys. Rev.* B **72** 085402